2024 IEEE/RSJ International Conference on Intelligent Robots and Systems (IROS)
October 14-18, 2024. Abu Dhabi, UAE

Online Adaptive Impedance Control with Gravity Compensation for an Interactive Lower-Limb Exoskeleton

Run Janna[1], Kanut Tarapongnivat[1], Natchaya Sricom[1], Chaicharn Akkawutvanich[1], Xiaofeng Xiong[2], and Poramate Manoonpong[1,2,*], *Senior Member*, *IEEE*

***Abstract*— While lower-limb exoskeletons have been increasingly used for gait assistance and rehabilitation, most of them continue to function as assistive devices in the exoskeleton-user relationship as a leader and follower. This limits the user's ability to interactively contribute to gait control. Therefore, this study proposes an interactive user-exoskeleton control strategy to translate the exoskeletons into interactive compliant companion devices with the exoskeleton-user relationship as the collaborator. This strategy is implemented through online adaptive impedance control with gravity compensation (OAIC-GC). It relies solely on internal pose feedback (joint position) rather than external sensors such as electromyography, torque, or force, as utilized in other assist-as-needed (AAN) control methods. The OAIC-GC can automatically capture the mechanical impedance dynamics of the user's lower limbs during walking and thus facilitate adaptive, versatile, and personalized gait assistance. It is evaluated using a real lower-limb exoskeleton system with six degrees of freedom (DOFs) across different users engaging in various activities. These activities include symmetrical and asymmetrical walking on a split-belt treadmill at different speeds, as well as walking up stairs. The results indicate a significant improvement in the exoskeleton's performance in terms of adaptability and movement smoothness under all activities when compared to traditional control. The proposed control reduces joint assistance torque across all exoskeleton joints, enhancing user interaction and comfort. This enables users to actively control their gait patterns, enabling the exoskeleton to operate in an interactive assist-as-needed (IAAN) mode.**

***Index Terms*— Variable compliant control, Wearable robots, Human-robot interaction, Gait rehabilitation.**

I. INTRODUCTION

Exoskeletons represent a promising advancement in the fields of rehabilitation, assistive devices, and human augmentation, offering hope for individuals with mobility impairments. Central to their effectiveness is the control mechanism, dictating their interaction with users and adaptation to environmental conditions. The use of these devices can facilitate motor recovery and functional independence, thus improving the quality of life for patients.

Traditional trajectory control (TC) involves the generation of predetermined joint positions or force trajectories to serve as reference commands for assistance or resistance. These trajectories are typically derived from pre-recordings of unimpaired individuals [1], those obtained during therapist-guided assistance [2], or by demonstration [3].

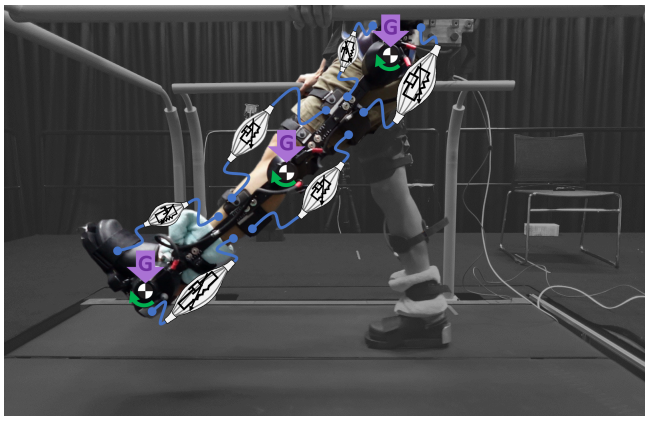

Fig. 1. The OAIC-GC control, comprising muscle-like compliance adaptation (white symbols) and gravity compensation (green arrows), leads to an interactive assist-as-needed control strategy. Here, G denotes gravity. Such implementation enhances the functionality of the EXO-H3 exoskeleton, enabling seamless interaction with users for gait assistance. By using the OAIC-GC control, the exoskeleton achieves advanced capabilities in generating adaptive assistance torque, adjusting its behavior in real time to ensure proper assistance and across various walking conditions.

In an effort to integrate lower-limb exoskeletons with gait assistance and rehabilitation, the focus has been on applying adaptive methods to minimize interaction forces between the exoskeleton and the user. These methods encompass the utilization of an adaptive frequency oscillator (AFO) [4], a support vector machine (SVM) [5], adaptive dynamic movement primitives (DMPs) [6], or central pattern generators (CPGs) coupled with premotor radial basis function networks (RBFN) [7]. However, these methods mainly detect and adapt gait frequency, potentially limiting the user's ability to actively engage in walking or rehabilitation.

To improve this, another control strategy known as assist-as-needed (AAN) for joint assistance torque adaptation based on impedance control (IC) or admittance control (AC) was introduced [8]. AAN-based control methods were used to support the specific needs according to the abilities of wearers. Most of the methods focus on compliance learning and adaptation to achieve effective AAN. These methods include variable admittance control (VAC), employing reinforcement learning (RL), to estimate admittance parameters relying on force sensors [9]. Other methods, such as variable

This work was supported by VISTEC through the EXOVIS Project under Grant I20POM-INT010 [PM] (*Corresponding author; e-mail: poramate.m@vistec.ac.th).

[1]R.J., K.T., N.S., C.A., and P.M. are with the Bio-inspired Robotics and Neural Engineering Laboratory, School of Information Science and Technology, Vidyasirimedhi Institute of Science and Technology (VISTEC), Rayong 21210, Thailand.

[2]X.X and P.M. are with the Embodied Artificial Intelligence and Neurorobotics Laboratory, SDU Biorobotics, the Mærsk Mc-Kinney Møller Institute, University of Southern Denmark (SDU), Odense 5230, Denmark.

impedance control (VIC), also utilize learning/optimization-based methods (e.g., neural network (NN) learning with the delta rule [10], particle swarm optimization (PSO) [11]) to estimate impedance parameters. However, it is important to note that all these methods require learning/optimization time and sample data to ensure their suitability for each individual. In other studies, adaptive impedance control has been introduced to diminish learning time and sample data requirements by incorporating state-of-the-art adaptive laws in various models. These models include utilizing fuzzy-based control (FBC) [12] based on inertial measurement unit (IMU) sensors, the combination of strength index (SI) and a generalized fuzzy hyperbolic model (GFHM) [13], or the use of fuzzy logic compliance adaptation and sliding mode control (FLCA-SM) [14].

The effectiveness of the aforementioned exoskeleton control methods varies depending on their respective approaches. In the VAC and VIC approaches [9]–[13], multiple sensors, such as joint encoders, plantar pressure or force, EMGs, IMUs, or their combination, are employed to estimate the admittance/impedance parameters to achieve the AAN strategy. However, the use of multiple sensor feedback requires complex signal processing, and the validation of exoskeleton-compliant behavior to accommodate treadmill speed changes and versatile gait assistance (i.e., asymmetrical walking and stair climbing) has not been demonstrated. Conversely, gait frequency adaptation methods [4]–[7] prioritize the adaptation of gait frequency but lack specific consideration for interaction force and compliance, resulting in a leader-follower operation mode rather than an interactive mode. Meanwhile, learning/optimization-based methods [9]–[11] necessitate long learning/optimization times and large sample data to determine the optimal parameters for individuals.

To address the research gaps in exoskeleton control, including the need for multiple sensory feedback, limited human involvement in the control loop, and long learning time or large sample data usage, this study introduces an online adaptive impedance control system with gravity compensation (OAIC-GC) for lower-limb exoskeletons. The OAIC-GC aims to redefine the role of exoskeletons in assistance and rehabilitation, translating them from functioning solely as assistive devices with the exo-user relationship as leader-follower to become interactive compliant companion (or interactive assist-as-needed, IAAN) devices with the exo-user relationship as the collaborator. To accomplish this, the OAIC-GC employs a simple joint angular position and velocity tracking error feedback to dynamically adjust the impedance and force control parameters, facilitating adaptive, personalized compliance. Additionally, it incorporates a model-based gravity compensator to enhance the level of adaptive exoskeleton assistance.

In a nutshell, the main contributions of this study are:

1) A novel IAAN control strategy combining online adaptive impedance control (OAIC) and gravity compensation (GC) to optimize joint assistance torques in a lower-limb exoskeleton. This real-time optimization enhances exo-user interaction for adaptive walking.
2) The OAIC mechanism capturing the mechanical impedance dynamics of the user's lower limbs with minimal sensory feedback from the exoskeleton's joint encoders. This enables practical, personalized, and compliant assistance.
3) Real-world validation demonstrating the superiority of the proposed control over traditional control across diverse walking conditions, including symmetrical, asymmetrical, and stair climbing, with multiple subjects.

II. System Overview

This section provides a comprehensive system overview of our control development and evaluation. The system consists of three main components: a lower-limb exoskeleton, interactive assist-as-needed control (OAIC-GC, see Section III),, and an adjustable speed split-belt treadmill (Fig. 2).

The lower-limb exoskeleton used in this study is the EXO-H3 developed by Technaid (Fig. 2). It has six active joints operating on the sagittal plane to assist the right and left hips (RH/LH), knees (RK/LK), and ankles (RA/LA) for gait assistance and rehabilitation. Each joint is driven by a smart electric actuator with a harmonic drive. Each actuator rotates forward/backward with a maximum operating torque of approximately 40 Nm and a peak torque of approximately 150 Nm. There are two sensors at each actuator: joint encoders and torque sensors. Additionally, there are four force sensors on each sole. Here, the joint position feedback is used in our control method for tracking error calculation, while the torque feedback is only used for the evaluation of the interaction torque between the exoskeleton and the user. The total weight of the exoskeleton is approximately 11 kg.

The split-belt treadmill used here is from Bertec. It is equipped with two side-by-side force plates, where each force plate provides six dimensions of load measurement (Fx, Fy, Fz, Mx, My, Mz). It can independently adjust the speed of each belt to simulate asymmetric walking conditions. Our developed GUI [15] enables real-time treadmill speed control and simultaneous recording of all feedback signals.

III. Interactive Assist-as-Needed Control Strategy

To achieve an interactive lower-limb exoskeleton (or companion device) driven by an interactive assist-as-needed control strategy, we developed online adaptive impedance control with gravity compensation (OAIC-GC, described in detail below). The control method is applied to control the joint assistance torques of the exoskeleton in accordance with the dynamic model described in Eq. (1):

$$\boldsymbol{M}(\boldsymbol{q})\ddot{\boldsymbol{q}} + \boldsymbol{C}(\boldsymbol{q},\dot{\boldsymbol{q}})\dot{\boldsymbol{q}} + \boldsymbol{G}(\boldsymbol{q}) = \boldsymbol{\tau}_c + \boldsymbol{\tau}_h + \boldsymbol{\tau}_{tm}, \quad (1)$$

where $\boldsymbol{q}$,$\dot{\boldsymbol{q}} \in \mathbb{R}^{6\times1}$ are joint angular positions and joint angular velocities of the six active joints of the exoskeleton. $\boldsymbol{M}(\boldsymbol{q}) \in \mathbb{R}^{6\times6}$ denotes a symmetric and positive definite inertia matrix. $\boldsymbol{C}(\boldsymbol{q},\dot{\boldsymbol{q}}) \in \mathbb{R}^{6\times6}$ represents the Coriolis and centrifugal matrix. $\boldsymbol{G}(\boldsymbol{q}) \in \mathbb{R}^{6\times1}$ is the gravitational effects matrix. $\boldsymbol{\tau}_c$, $\boldsymbol{\tau}_h$, and $\boldsymbol{\tau}_{tm} \in \mathbb{R}^{6\times1}$ describe the joint assistance

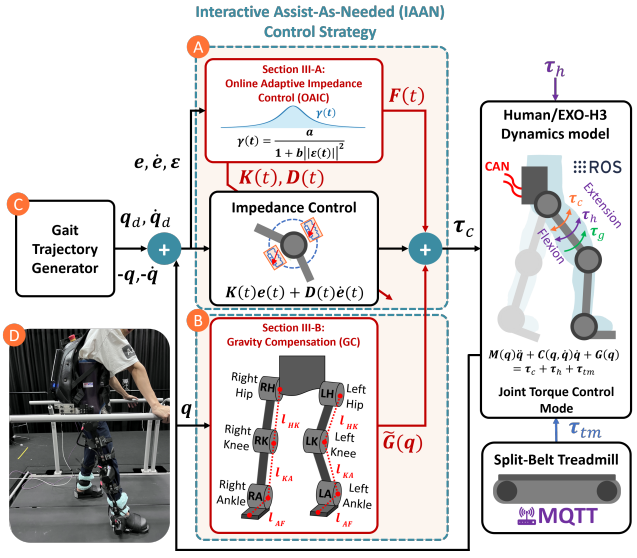

Fig. 2. An overview of the system setup for developing an interactive exoskeleton and demonstrating its performance during gait assistance at different treadmill speeds. The setup includes the online adaptive impedance control system with gravity compensation (OAIC-GC, shown in (A) and (B)), the gait trajectory generator (shown in (C)), an adjustable speed split-belt treadmill (Bertec), and a lower-limb exoskeleton (EXO-H3, shown in (D)). The communications of the system are done using the robotic operating system (ROS) for the OAIC-GC control, MQTT for the treadmill speed control, and controller area network (CAN) for the EXO-H3 low-level joint torque control (see [15] for more detail).

torques, external human torques, and external torques from the environment (e.g., treadmill), respectively.

A. Online Adaptive Impedance Control (OAIC)

According to Eq. (1), the joint assistance torques ($\boldsymbol{\tau}_c \in \mathbb{R}^{6\times1}$) for controlling the exoskeleton are generated by feedback and feedforward terms according to:

$$\boldsymbol{\tau}_c = \underbrace{\boldsymbol{K}(t)\boldsymbol{e}(t) + \boldsymbol{D}(t)\dot{\boldsymbol{e}}(t)}_{\text{feedback}} + \underbrace{\boldsymbol{F}(t) + \tilde{\boldsymbol{G}}(\boldsymbol{q})}_{\text{feedforward}}. \tag{2}$$

The feedback part is based on impedance control where both stiffness ($\boldsymbol{K}(t) \in \mathbb{R}^{6\times6}$) and damping ($\boldsymbol{D}(t) \in \mathbb{R}^{6\times6}$) parameters are adapted online. The feedforward part is a combination of the force term ($\boldsymbol{F}(t) \in \mathbb{R}^{6\times1}$) and gravity compensation term ($\tilde{\boldsymbol{G}}(\boldsymbol{q}) \in \mathbb{R}^{6\times1}$). This feedforward term serves to enhance tracking performance and compensate for the effects of gravity on the structure of the exoskeleton (see Fig. 2 and Section III-B). It should be noted that the first three terms correspond to the OAIC mechanism, whereas the last term corresponds to the GC mechanism.

$\boldsymbol{e}(t), \dot{\boldsymbol{e}}(t) \in \mathbb{R}^{6\times1}$ represent the joint angular position and velocity errors, respectively. They are given by:

$$\begin{gathered}\boldsymbol{e}(t) = \boldsymbol{q}_d(t) - \boldsymbol{q}(t), \dot{\boldsymbol{e}}(t) = \dot{\boldsymbol{q}}_d(t) - \dot{\boldsymbol{q}}(t), \\ \boldsymbol{\varepsilon}(t) = \boldsymbol{e}(t) + \beta\dot{\boldsymbol{e}}(t),\end{gathered} \tag{3}$$

where $\boldsymbol{q}_d(t), \dot{\boldsymbol{q}}_d(t) \in \mathbb{R}^{6\times1}$ are the desired joint angular position and velocity profiles of the six actuators provided by the default gait trajectory generator of EXO-H3. It should be noted that the gait trajectory generator is not the focus of this study; therefore, it is not described here. However, we refer to [7] for more detail. $\boldsymbol{\varepsilon}(t) \in \mathbb{R}^{6\times1}$ denotes the joint tracking error with factor $\beta = 0.05$.

The adaptation mechanism will be optimized by the concurrent minimization of two cost functions: the compliance efforts ($\boldsymbol{J}_c(t)$) and the motion error ($\boldsymbol{J}_p(t)$) to maintain control stability with minimal tracking error according to:

$$\begin{gathered}\boldsymbol{J}_o(t) = \boldsymbol{J}_c(t) + \boldsymbol{J}_p(t), \\ \boldsymbol{J}_c(t) = \frac{1}{2}\int_{t-T}^{t} (\boldsymbol{K}(\sigma))^2 + (\boldsymbol{D}(\sigma))^2 + (\boldsymbol{F}(\sigma))^2 d\sigma, \\ \boldsymbol{J}_p(t) = \int_{t-T}^{t} \dot{\boldsymbol{V}}(\sigma)d\sigma, \boldsymbol{V}(t) = \frac{1}{2}\boldsymbol{\varepsilon}^T(t)\boldsymbol{M}(\boldsymbol{q})\boldsymbol{\varepsilon}(t).\end{gathered} \tag{4}$$

This co-minimization leads to the adaptation of the lower-limb exoskeleton joint impedance and force, as shown in Eq.(5):

$$\begin{gathered}\boldsymbol{K}(t) = \boldsymbol{F}(t)\boldsymbol{e}^T(t), \boldsymbol{D}(t) = \boldsymbol{F}(t)\dot{\boldsymbol{e}}^T(t), \boldsymbol{F}(t) = \frac{\boldsymbol{\varepsilon}(t)}{\boldsymbol{\gamma}(t)}, \\ \boldsymbol{\gamma}(t) = \frac{a}{1 + b||\boldsymbol{\varepsilon}(t)||^2},\end{gathered} \tag{5}$$

where $\boldsymbol{\gamma}(t)$ is an adaptation term with positive scalars $a > 0$ and $b > 0$. The values of a and b can be selected depending on the desired rate of adaptive response. In this study, a and b are set to $a = 0.2$ and $b = 5$. These values and adaptation law (Eq. (5)) are based on human muscle-inspired impedance adaptation control (see [16] for more detail).

B. Gravity Compensation (GC)

According to Eq. (2), $\tilde{\boldsymbol{G}}(\boldsymbol{q})$ describes the required torques to counteract the effects of gravity on the exoskeleton joints, represented as:

$$\tilde{\boldsymbol{G}}(q) = \begin{bmatrix}\tau_{g_{RH}} & \tau_{g_{RK}} & \tau_{g_{RA}} & \tau_{g_{LH}} & \tau_{g_{LK}} & \tau_{g_{LA}}\end{bmatrix}^T, \tag{6}$$

where $\tau_{g_{RH}}$, $\tau_{g_{RK}}$, $\tau_{g_{RA}}$, $\tau_{g_{LH}}$, $\tau_{g_{LK}}$, and $\tau_{g_{LA}}$ are the gravity compensation joint torques of the right hip, right knee, right ankle, left hip, left knee, and left ankle joints, respectively. By modeling the exoskeleton limb as a triple pendulum [17] and applying the Lagrangian dynamics approach, the gravity compensation joint torques can be obtained as follows:

$$\begin{aligned}\tau_{g_{RH}} &= m_K g \cdot (l_{HK}\sin(q_{RH}(t))) \\ &+ m_A g \cdot (l_{HK}\sin(q_{RH}(t)) + l_{KA}\sin(q_{RH}(t) + q_{RK}(t))) \\ &+ m_F g \cdot (l_{HK}\sin(q_{RH}(t)) + l_{KA}\sin(q_{RH}(t) + q_{RK}(t)) \\ &+ l_{AF}\sin(q_{RH}(t) + q_{RK}(t) + q_{RA}(t))),\end{aligned} \tag{7}$$

$$\begin{aligned}\tau_{g_{LH}} &= m_K g \cdot (l_{HK}\sin(q_{LH}(t))) \\ &+ m_A g \cdot (l_{HK}\sin(q_{LH}(t)) + l_{KA}\sin(q_{LH}(t) + q_{LK}(t))) \\ &+ m_F g \cdot (l_{HK}\sin(q_{LH}(t)) + l_{KA}\sin(q_{LH}(t) + q_{LK}(t)) \\ &+ l_{AF}\sin(q_{LH}(t) + q_{LK}(t) + q_{LA}(t))),\end{aligned} \tag{8}$$

$$\begin{aligned}\tau_{g_{RK}} &= m_A g \cdot (l_{KA}\sin(q_{RH}(t) + q_{RK}(t))) \\ &+ m_F g \cdot (l_{KA}\sin(q_{RH}(t) + q_{RK}(t)) \\ &+ l_{AF}\sin(q_{RH}(t) + q_{RK}(t) + q_{RA}(t))),\end{aligned} \tag{9}$$

$$\begin{aligned}\tau_{g_{LK}} &= m_{A} g \cdot (l_{KA} \sin(q_{LH}(t) + q_{LK}(t))) \\ &+ m_{F} g \cdot (l_{KA} \sin(q_{LH}(t) + q_{LK}(t)) \\ &+ l_{AF} \sin(q_{LH}(t) + q_{LK}(t) + q_{LA}(t))),\end{aligned} \tag{10}$$

$$\tau_{g_{RA}} = m_{F} g \cdot (l_{AF} \sin(q_{RH}(t) + q_{RK}(t) + q_{RA}(t))), \tag{11}$$

$$\tau_{g_{LA}} = m_{F} g \cdot (l_{AF} \sin(q_{RH}(t) + q_{RK}(t) + q_{RA}(t))), \tag{12}$$

where $q_{RH}(t)$, $q_{RK}(t)$, $q_{RA}(t)$, $q_{LH}(t)$, $q_{LK}(t)$, and $q_{LA}(t)$ are the joint angular positions of the right hip, right knee, right ankle, left hip, left knee, and left ankle joints, respectively. $m_{K} = 1.5$ kg, $m_{A} = 1.5$ kg, and $m_{F} = 0.8$ kg denote the masses of the knee and ankle joints and the exoskeleton foot part, respectively (Fig. 2). g represents the gravitational acceleration ($9.8\ m/s^2$). The link length is defined as follows: l_{HK} for hip to knee, l_{KA} for knee to ankle, and l_{AF} for ankle to foot (see Table I). Note that the EXO-H3 links can be manually adjusted for individual subjects. The effect of implementing the gravity compensation term can be seen at https://youtu.be/oBkiOZryvBg.

IV. Experiments and Results

This section presents the three main experiments conducted to assess the performance of the OAIC-GC. The first experiment investigated the OAIC-GC adaptability along with user-exoskeleton interaction under rapid changes in treadmill speed. The second experiment examined the OAIC-GC adaptability and user-exoskeleton interaction under multiple treadmill speeds and investigated the operating range of the OAIC-GC. Both experiments were performed on two healthy subjects (S1 and S2 in Table I). Additionally, the final experiment demonstrated the performance of the OAIC-GC for versatile gait assistance across a variety of activities. We also compared the performance of the OAIC-GC with the traditional trajectory control (TC)[1] typically used for the EXO-H3. Note that the experiment was approved by the Research Ethics Committee from the University of Southern Denmark, Odense, Denmark (Case no. 20/70422).

TABLE I
Details of the healthy subjects in this study

Subjects	Gender	Weight (kg)	Height (cm)	l_{HK} (cm)	l_{KA} (cm)	l_{AF} (cm)
S1	Male	60	175	48	45	30
S2	Male	70	170	45	45	30

A. Adaptability under Rapid Changes in Treadmill Speed

In the first experiment, two subjects walked on the treadmill while wearing the EXO-H3 with a predefined gait trajectory provided by the gait trajectory generator (Fig. 2).

At the beginning (t = 0 s), the treadmill speed was set to 0.27 m/s for slow speed, and the gait frequency set to 0.256 Hz for slow walking by the gait trajectory generator to match the treadmill speed. Subsequently, at t = 20 s, the treadmill speed was rapidly changed to a fast speed of 0.63 m/s (approximately 130% speed increase), while the gait trajectory remained at the slow gait frequency. This fast treadmill speed lasted for 20 s, after which the experiment was terminated. The experiment was repeated five times for each control method and subject.

Figure 3(A) and (C) depict the results for walking at slow and fast treadmill speeds, respectively. The vertical axis denotes the joint angles of the right leg, while the horizontal axis describes the ratio of the gait cycle, varying from 0 to 1. This cycle encompasses various phases, including the heel strike (HS), toe-off (TO), stance (ST), and swing (SW) phases. The gait cycle time window was detected by the foot force sensors of the EXO-H3, which also captured instances of falling off the treadmill.

The first row shows the change in the right hip joint over one gait cycle. In the context of slow treadmill speed, both TC and OAIC-GC exhibit minimal deviations from the desired gait trajectory. In the case of fast treadmill speed, the TC demonstrates a slightly greater deviation from the desired gait trajectory, while the OAIC-GC displays a significant divergence in extension and flexion beyond the desired trajectory during the ST and SW phases.

The second row shows the change in the right knee joint over one gait cycle. During slow treadmill speed, the TC demonstrates a slight right shift away from the desired trajectory at the TO phase. In contrast, the OAIC-GC has a slightly more rightward shift than the TC during the same TO phase. During fast treadmill speed, the OAIC-GC shows a slight variation with more flexion during the SW phase compared to the OAIC-GC during the period of slow speed due to the increasing speed of the treadmill. In contrast, the TC exhibits a lower peak and substantial deviation (indicated by the red-shaded region) at the TO phase. This indicates that the TC does not permit an increase in the flexion of the knee joint when the speed of the treadmill is increased.

The third row shows the change in the right ankle joint over one gait cycle. During slow treadmill speed, the TC exhibits a moderate rightward deviation from the desired trajectory, while the OAIC-GC has a more pronounced shift to the right compared to the TC. When operating at a fast treadmill speed, the TC shows a similar deviation to that observed during slow treadmill speed, while the OAIC-GC exhibits greater flexion at the SW phase compared to the slow treadmill speed period.

Figure 3(B) and (D) depict the percentage of compliance deviation in joint angles ($\%\bar{c}_j^i$). This metric serves as an indicator of joint flexibility and is determined through the application of the measurement equation:

$$\%\bar{c}_j^i = \frac{\frac{\sum_{t=0}^{N} |q_{d,j}^i(t) - q_j^i(t)|}{N}}{|\max(q_{d,j}^i) - \min(q_{d,j}^i)|} \times 100, \tag{13}$$

where j represents the specific six joints of the exoskeleton, and i represents a slow or fast treadmill speed. N represents the number of time steps (here $N = 40 \times 10^3$ for a 40-second experiment). $q_{d,j}^i(t)$ and $q_j^i(t)$ denote the desired and

[1]Note that the trajectory control utilizes high constant stiffness ($\boldsymbol{K} = 10$) and damping ($\boldsymbol{D} = 100$) parameters specifically tuned for the precise tracking of gait trajectories, while the OAIC-GC employs dynamically adjustable stiffness ($\boldsymbol{K}(t)$) and damping ($\boldsymbol{D}(t)$) parameters (Eq.(5)).

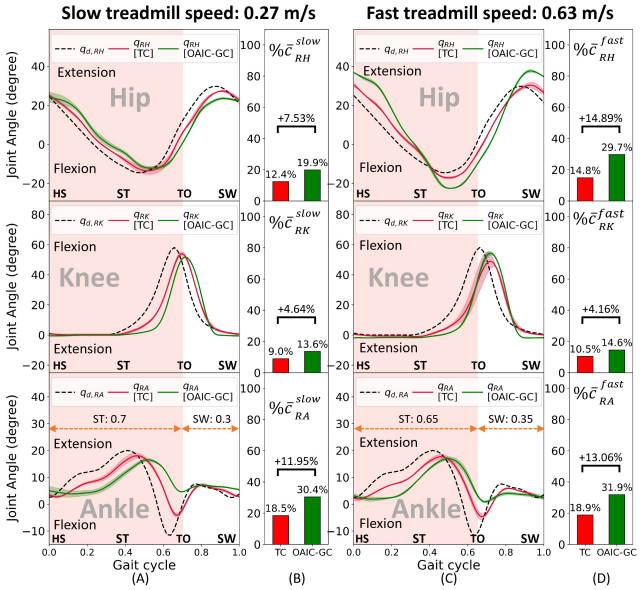

Fig. 3. Hip (top), knee (middle), and ankle (bottom) joint angle feedback from the EXO-H3 of the right leg observed during walking at the slow (A) and fast (C) treadmill speeds. A similar behavior in joint angle feedback of the left leg is not shown. Each graph in (A) and (C) presents the joint angle feedback from the OAIC-GC (green line) and TC (red line) over one gait cycle. The desired joint trajectories generated by the gait trajectory generator are shown in black dashed lines. The red background indicates the stance (ST) phase, while the white background represents the swing (SW) phase. HS and TO denote the heel-strike and toe-off phases, respectively. (B) and (D) illustrate the compliance deviation joint angles as percentage bars during walking at the slow and fast treadmill speeds, respectively. Joint trajectories (black dashed lines) were generated for slow walking and applied to both slow and fast treadmill speeds. This demonstrates the adaptability of the OAIC-GC, allowing the user to contribute to exoskeleton control for online walking speed adjustment, even with preset joint trajectories (or gait trajectory). This capability ensures stable walking, defined as the ability to walk on the treadmill at various speeds without falling.

actual joint angular positions, respectively, according to the fast or slow treadmill speed (i) and all joints (j). $\max(q^i_{d,j})$ and $\min(q^i_{d,j})$ represent the maximum and minimum values of the desired joint angular position, respectively, indicating the peak-to-peak range. The percentage of compliance deviation in joint angles emphasizes notably higher joint compliance in the OAIC-GC compared to the TC at both slow and fast treadmill speeds. The higher the percentage, the greater the contribution of the user in controlling the exoskeleton, demonstrating a 7.53% increase in hip joints, 4.64% in knee joints, and 11.95% in ankle joints compared to traditional trajectory control at a slow treadmill speed, and 14.89%, 4.16%, and 13.06% in hip, knee and ankle joints, respectively, at a fast treadmill speed. In other words, the exoskeleton operates in an interactive collaborator mode rather than a stiff leader-follower mode.

Figure 4 shows snapshots of walking behavior under slow and fast treadmill speeds controlled by the OAIC-GC or TC. With the OAIC-GC, there is a distinct deviation in joint angles, allowing subjects to extend their steps and change walking speed within predefined gait trajectory. This ensures stable walking , particularly at the fast treadmill speed. On the contrary, the TC restricts subjects from extending their

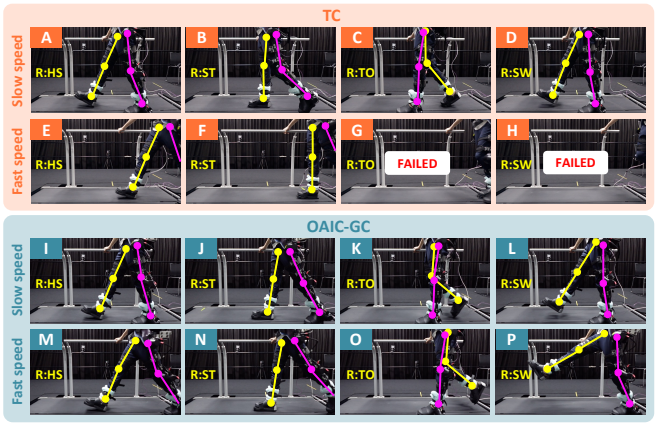

Fig. 4. Time-series snapshots of subject S1. A yellow visual skeleton represents the right leg of the exoskeleton, while a pink visual skeleton represents the left leg. The yellow text within the segment indicates the different phases of the gait cycle, specifically on the right leg (R: right, HS: heel strike, ST: stance, TO: toe off, SW: swing). FAILED refers to the subject sliding off the treadmill. (A)-(D) and (I)-(L) demonstrate the walking behavior controlled by the TC and OAIC-GC, respectively, under the slow treadmill speed (0.27 m/s). (E)-(H) and (M)-(P) represent the walking behavior controlled by the TC and OAIC-GC, respectively, under the fast treadmill speed (0.63 m/s). A video of this experiment can be seen at https://www.manoonpong.com/OAICGC/video.mp4, starting at 35 seconds.

steps beyond the predefined gait trajectory, especially when faced with the fast treadmill speed. This is due to the constant stiffness and damping parameters of the TC, acting as stiff TC control. This limitation results in subjects deviating and eventually shifting from the treadmill, as illustrated in Fig. 4(E)-(H).

A further analysis via the joint assistance torque (τ_c) throughout one gait cycle is depicted in Fig. 5. The first row illustrates the dynamics of the joint assistance torque of the right hip joint. At slow treadmill speed, the OAIC-GC generates a smooth and consistent torque profile, a reduction of 52.25% of the maximum standard deviation compared to the TC. Conversely, at fast treadmill speed, the OAIC-GC produces a notably consistent torque profile, reducing 74.61% of the maximum standard deviation compared to the TC at the TO and HS phases.

The second row illustrates the dynamics of the joint assistance torque of the right knee joint. At slow treadmill speed, OAIC-GC exhibits a maximum standard deviation reduction of 25.57%, despite both the TC and OAIC-GC showing similar peak torques at the SW phase. However, OAIC-GC demonstrates a larger reduction of 65.20% at fast treadmill speed compared to the TC, at TO and HS phases.

The third row illustrates the dynamics of the joint assistance torque of the right ankle joint. At the slow treadmill speed, the OAIC-GC shows a slight increase in the maximum standard deviation of 14.97% compared to the TC in the SW and ST phases. At the fast treadmill speed, the OAIC-GC maintains a relatively consistent torque profile with a maximum standard deviation reduction of 69.29% compared to the TC. Meanwhile, the TC demonstrates a pronounced decrease in torque peak and a significant increase in torque

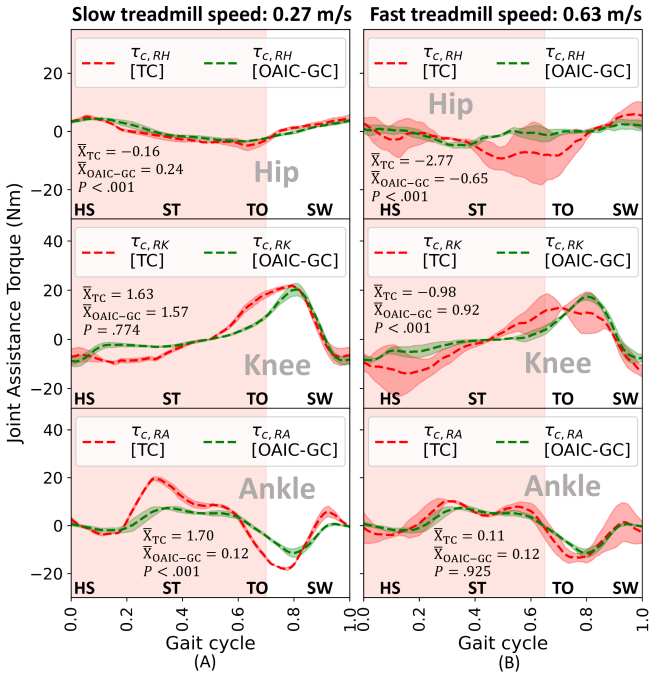

Fig. 5. Joint assistance torque (τ_c) of the right hip, right knee, and right ankle joints of the EXO-H3 under the TC (red) and OAIC-GC (green) over one gait cycle. (A) Walking at the slow treadmill speed. (B) Walking at the fast treadmill speed. The red background indicates the stance (ST) phase, while the white background represents the swing (SW) phase. HS and TO denote the heel-strike and toe-off phases, respectively. *P*-values for differences between methods were calculated using Welch's t-test.

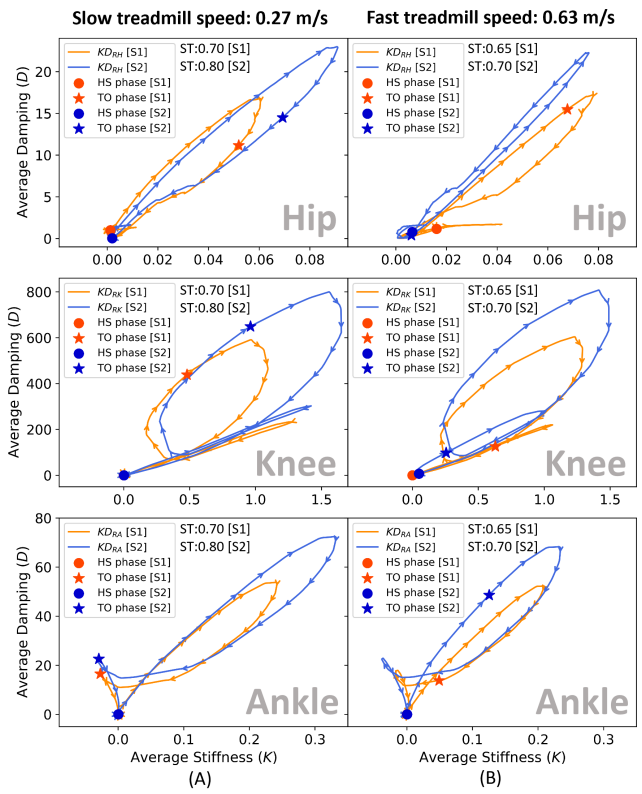

Fig. 6. Impedance loops in the right leg joints of two subjects (S1: orange, S2: blue). Each loop illustrates the average stiffness (horizontal axis) and average damping (vertical axis) across one gait cycle. (A) Walking at the slow treadmill speed. (B) Walking at the fast treadmill speed. Arrows indicate the direction of the impedance loop aligned with the gait cycle, segmented into the HS (circle) and TO (star) phases. ST indicates the stance phase ratios for the two subjects (S1 and S2).

deviation throughout the gait cycle. It should be noted that the maximum standard deviation indicates the consistency and smoothness of the torque profile within one gait cycle.

Accordingly, when comparing the root mean square (RMS) of joint assistance torques during walking at the slow treadmill speed, the OAIC-GC exhibits lower RMS values than the TC in hip, knee, and ankle assistance torques, with reductions of 13.42%, 27.19%, and 49.21%, respectively. The same trend was also observed during walking at the fast treadmill speed, with the OAIC-GC demonstrating lower RMS values in hip, knee, and ankle assistance torques compared to the TC, with reductions of 58.94%, 31.03%, and 24.67%, respectively. The lower RMS values of the OAIC-GC imply its capability to produce more consistent, smooth, and essential torques for interactive assist-as-needed control. This can enhance user comfort and enable natural interaction with the exoskeleton. Additionally, the OAIC-GC can accommodate a mismatch between gait frequency and treadmill speed (e.g., slow gait frequency and fast treadmill speed) by allowing subjects to walk without generating excessive torque, thereby ensuring consistent joint assistance torque behavior.

Figure 6 illustrates the adaptive stiffness and damping behavior quantified through the impedance loop. Figure 6(A) illustrates the characteristics of the impedance loops of all joints for two subjects during walking at the slow treadmill speed. Comparable patterns can be observed for both subjects, indicated by similar loops and the locations of HS and TO phases within the impedance loops. However, only the loop size differs between subjects. Subject S2 exhibits higher stiffness and damping value utilization across all three joints, resulting in larger loop sizes. Figure 6(B) illustrates the characteristics of the impedance loops during walking at the fast treadmill speed. The impedance loops of all joints for both subjects show quite similar patterns compared to the slow treadmill speed condition. Only the loop sizes differ. This analysis demonstrates the capability of the OAIC-GC in dynamically adapting its impedance requirements to all joints during walking for individual subjects (S1 and S2), thereby resulting in adaptive personalized gait assistance.

B. Adaptability under Multiple Treadmill Speeds

In the second experiment, two subjects walked on the treadmill while wearing the EXO-H3 with a predefined gait trajectory set at a normal treadmill speed of 0.38 m/s. Accordingly, the gait trajectory generator produced a default gait pattern with a frequency of 0.333 Hz to match the treadmill speed. Throughout the experiment, the treadmill speed was initially set to normal and then gradually adjusted by increasing and decreasing by 20%, 40%, 60%, and 80%, while the gait frequency from the gait trajectory generator remained unchanged. The success rate was determined by

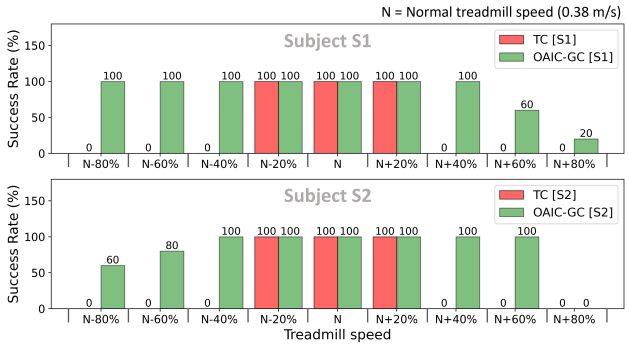

Fig. 7. Success rate of walking under multiple treadmill speeds. The treadmill speed is increased and decreased by 20%, 40%, 60%, and 80% of its normal speed (0.38 m/s). The success rate is expressed as a percentage for both subject S1 (upper row) and subject S2 (lower row) under the OAIC-GC (green) and TC (red).

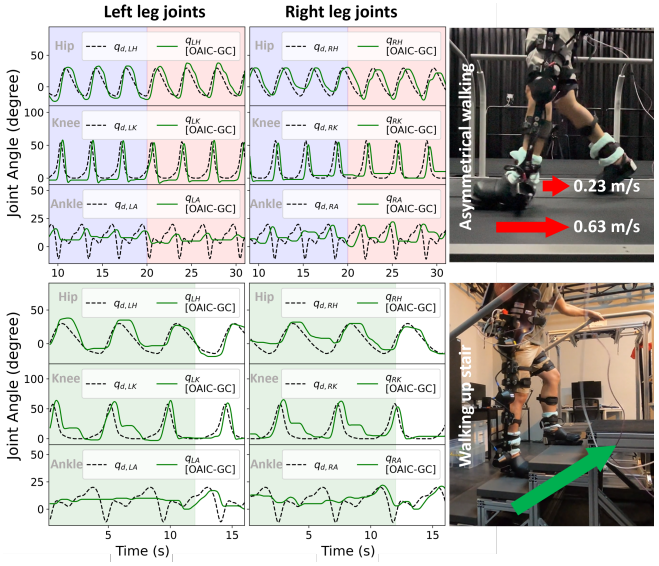

Fig. 8. Versatile gait assistance. The symmetrical and asymmetrical walking experiment is shown at the top (see also https://www.manoonpong.com/OAICGC/video.mp4, starting at 1 minute and 24 seconds). The blue and red backgrounds denote symmetrical walking and asymmetrical walking, respectively. The walking-up-stairs experiment is shown at the bottom (see also https://www.manoonpong.com/OAICGC/video.mp4, starting at 2 minutes and 5 seconds). The green and white backgrounds denote walking upstairs and on level ground, respectively. The green line represents the joint angle feedback from the OAIC-GC. The black dashed line indicates the desired joint trajectory produced by the gait trajectory generator.

each subject's ability to complete the entire 40-second experimental session without falling off the treadmill. "Falling off" was defined as deviating from the starting point by more than 50 cm. This evaluation was performed for both control methods (OAIC-GC and TC). The experiment was repeated five times for each control method and subject. Figure 7 displays the success rates achieved by the OAIC-GC and TC. It is evident that the OAIC-GC can operate within a range of ±80% of the normal treadmill speed, which is noticeably larger than the TC's range of ±20% of the normal treadmill speed. This highlights the OAIC-GC's superior capability in enabling subjects to deal with multiple treadmill speeds without requiring a change in gait frequency.

C. Adaptability for Versatile Gait Assistance

In the final experiment, we demonstrated the adaptability of the OAIC-GC for versatile gait assistance in symmetrical walking, asymmetrical walking, and walking up stairs. To set up symmetrical and asymmetrical walking conditions, a subject walked on the treadmill while wearing the EXO-H3 with the predefined gait trajectory and frequency (0.33 Hz) set for a normal treadmill speed of 0.38 m/s. Initially, both the left and right belt speeds of the treadmill were set equally at 0.38 m/s, simulating a symmetrical walking condition. After approximately 20 seconds, the left belt speed was increased to 0.63 m/s, and the right one decreased to 0.23 m/s, simulating an asymmetrical walking condition. The same gait trajectory and frequency (0.33 Hz) were used for walking up stairs.

Figure 8 illustrates the experimental results. As can be observed, the subject successfully walked on the treadmill under both symmetrical and asymmetrical conditions, as well as walked up stairs. The subject effectively collaborated with the exoskeleton and contributed to its control for gait adaptation to deal with varying right-left belt speeds. Interestingly, owing to the adaptive compliance of the OAIC-GC, the subject was also able to shape the predefined walking gait to seamlessly transition into a stair-climbing gait, an interactive ability not achievable with the TC.

V. Discussion and Conclusion

A novel interactive assist-as-needed control strategy is proposed in this study, implemented through the OAIC and GC mechanisms, for an interactive lower-limb exoskeleton. It aims to optimize assistance for the user while focusing on adapting to individual flexibility and compensating for the effects of gravity, as outlined in Eqs. (2)-(12). Moreover, the adaptation law, as described in Eq. (5), relies only on the simple joint angular position and velocity tracking error feedback derived from the exoskeleton's joint encoders. Notably, this approach avoids the necessity for additional sensor systems, such as IMUs [12], EMG [10], or force/torque sensors [12], [13], thereby simplifying the system setup on both the user and exoskeleton. The OAIC-GC allows for the quantification and characterization of mechanical impedance, depending on the assistance requirements of each user during walking, resulting in personalized gait assistance (Fig. 6).

In comparison to other related AAN control methods (see Table II), our interactive AAN control method enables users to adapt well to various treadmill speeds without altering gait frequency or phase adaptation (see Fig. 7). Moreover, it is not merely restricted to level floor walking but also accommodates different scenarios, such as asymmetrical walking and stair climbing (see Fig. 8). The ability to handle a variety of activities under a given gait trajectory has not been demonstrated by others [9]–[13]. Our method can immediately online adapt impedance parameters based solely on the joint tracking error (Eq. (3)) without the need for large sample data or a long learning time. In contrast,

TABLE II

A COMPARISON BETWEEN DIFFERENT STATE-OF-THE-ART ASSIST-AS-NEEDED (AAN) CONTROL METHODS AND OUR PROPOSED METHOD

Method	CS	AJ	SF	TR	D
RL [9]	VAC	H, K (4DOFs)	J, F	✓	D1
NN [10]	VIC	H, K, A (6DOFs)	J, EMG	✓	D1
PSO [11]	VIC	K (2DOFs)	J	✓	D1
FBC [12]	VIC	H, K (4DOFs)	J, IMU, F	✗	D1, D2
SI-GFHM [13]	VIC	H (2DOFs)	J, T	✗	D1
OAIC-GC (OURS)	OAVIC	H, K, A (6DOFs)	J	✗	D1-D4

CS: Control strategy, AJ: Actuated joint, DOFs: Degrees of freedom, SF: Sensory feedback, TR: Training time and data samples requirements, D: Demonstrations, VAC: Variable admittance control, VIC: Variable impedance control, OAVIC: Online adaptive variable impedance control, H: Hip, K: Knee, A: Ankle, J: Joint encoders, F: Force sensors, EMG: Electromyography sensors, T: Torque sensors, IMU: Inertial measurement unit, D1: Symmetrical walking, D2: Walking on different treadmill speeds, D3: Asymmetrical walking, D4: Walking up stairs. ✓and ✗ denote inclusion, and exclusion.

most adaptive mechanisms utilize a learning-based approach to approximate the impedance and admittance parameters to achieve an AAN control strategy. The approach requires training the model using large amounts of sample data or simulations [9]–[11]. Consequently, this becomes impractical, and the learned parameters may not be directly applicable to new (unseen) users or environments. While some methods can achieve online adaptive interaction control for adapting impedance, admittance, or joint assistance torque parameters without requiring a training process, they still rely on complex sensory feedback, such as EMG, joint interaction torque, and/or force feedback [10], [12], [13].

The control method in this study is demonstrated on healthy subjects. However, it has potential applicability to non-ambulatory subjects with muscle weakness down to grade 3[2] (personal communication with orthopedic doctors and physiotherapists). Future work will involve clinical validation of the control method, integration of gait frequency and pattern adaptation mechanisms [7] for extending its operating range, and investigation of ankle inversion and eversion control for lateral walking stability and balance enhancement [18].

[2]The subject can move against gravity, but not against added resistance.

REFERENCES

[1] J. S. Lora-Millan, F. J. Sanchez-Cuesta, J. P. Romero, J. C. Moreno, and E. Rocon, "A unilateral robotic knee exoskeleton to assess the role of natural gait assistance in hemiparetic patients," *Journal of NeuroEngineering and Rehabilitation*, vol. 19, no. 1, p. 109, Oct 2022. [Online]. Available: https://doi.org/10.1186/s12984-022-01088-2

[2] M. D. S. Manchola, L. J. A. Mayag, M. Munera, and C. A. C. García, "Impedance-based backdrivability recovery of a lower-limb exoskeleton for knee rehabilitation," in *2019 IEEE 4th Colombian Conference on Automatic Control (CCAC)*, 2019, pp. 1–6.

[3] L. Luo, M. J. Foo, M. Ramanathan, J. K. Er, C. H. Chiam, L. Li, W. Y. Yau, and W. T. Ang, "Trajectory generation and control of a lower limb exoskeleton for gait assistance," *Journal of Intelligent & Robotic Systems*, vol. 106, no. 3, p. 64, Nov 2022. [Online]. Available: https://doi.org/10.1007/s10846-022-01763-5

[4] H. Talatian, M. Karami, H. Moradi, and G. Vossoughi, "Design and implementation of an intelligent control system for a lower-limb exoskeleton to reduce human energy consumption," in *2021 10th International Conference on Modern Circuits and Systems Technologies (MOCAST)*, 2021, pp. 1–4.

[5] K. Seo, K. Kim, Y. J. Park, J.-K. Cho, J. Lee, B. Choi, B. Lim, Y. Lee, and Y. Shim, "Adaptive oscillator-based control for active lower-limb exoskeleton and its metabolic impact," in *2018 IEEE International Conference on Robotics and Automation (ICRA)*, 2018, pp. 6752–6758.

[6] S. Qiu, W. Guo, F. Zha, J. Deng, and X. Wang, "Exoskeleton active walking assistance control framework based on frequency adaptive dynamics movement primitives," *Frontiers in Neurorobotics*, vol. 15, 2021. [Online]. Available: https://www.frontiersin.org/articles/10.3389/fnbot.2021.672582

[7] C. Akkawutvanich and P. Manoonpong, "Personalized symmetrical and asymmetrical gait generation of a lower limb exoskeleton," *IEEE Transactions on Industrial Informatics*, vol. 19, no. 9, pp. 9798–9808, Sep. 2023, publisher Copyright: © 2005-2012 IEEE.

[8] R. Baud, A. R. Manzoori, A. Ijspeert *et al.*, "Review of control strategies for lower-limb exoskeletons to assist gait," *Journal of NeuroEngineering and Rehabilitation*, vol. 18, no. 1, p. 119, 2021.

[9] G. Bingjing, H. Jianhai, L. Xiangpan, and Y. Lin, "Human–robot interactive control based on reinforcement learning for gait rehabilitation training robot," *International Journal of Advanced Robotic Systems*, vol. 16, no. 2, p. 1729881419839584, 2019. [Online]. Available: https://doi.org/10.1177/1729881419839584

[10] F. Zhang, Z.-G. Hou, L. Cheng, W. Wang, Y. Chen, J. Hu, L. Peng, and H. Wang, "ileg—a lower limb rehabilitation robot: A proof of concept," *IEEE Transactions on Human-Machine Systems*, vol. 46, no. 5, pp. 761–768, 2016.

[11] G. V. Ali Taherifar and A. S. Ghafari, "Optimal target impedance selection of the robot interacting with human," *Advanced Robotics*, vol. 31, no. 8, pp. 428–440, 2017. [Online]. Available: https://doi.org/10.1080/01691864.2016.1272491

[12] H. T. Tran, H. Cheng, H. Rui, X. Lin, M. K. Duong, and Q. Chen, "Evaluation of a fuzzy-based impedance control strategy on a powered lower exoskeleton," *International Journal of Social Robotics*, vol. 8, no. 1, pp. 103–123, Jan 2016. [Online]. Available: https://doi.org/10.1007/s12369-015-0324-9

[13] N. Naghavi, A. Akbarzadeh, S. M. Tahamipour-Z., and I. Kardan, "Assist-as-needed control of a hip exoskeleton based on a novel strength index," *Robotics and Autonomous Systems*, vol. 134, p. 103667, 2020. [Online]. Available: https://www.sciencedirect.com/science/article/pii/S0921889020305078

[14] B. Zhong, J. Cao, K. Guo, A. McDaid, Y. Peng, Q. Miao, S. Xie, and M. Zhang, "Fuzzy logic compliance adaptation for an assist-as-needed controller on the gait rehabilitation exoskeleton (garex)," *Robotics and Autonomous Systems*, vol. 133, p. 103642, 2020. [Online]. Available: https://www.sciencedirect.com/science/article/pii/S0921889020304826

[15] N. Sricom, W. Ketrungsri, C. Akkawutvanich, and P. Manoonpong, "Vistec-gait: A versatile automated gait lab system for closed-loop robotic exoskeleton assisted rehabilitation," in *2024 IEEE/SICE International Symposium on System Integration (SII)*, 2024, pp. 1024–1025.

[16] X. Xiong and P. Manoonpong, "Adaptive motor control for human-like spatial-temporal adaptation," in *2018 IEEE International Conference on Robotics and Biomimetics (ROBIO)*, 2018, pp. 2107–2112.

[17] B. Yesilyurt, "Equations of motion formulation of a pendulum containing n-point masses," *arXiv preprint arXiv:1910.12610*, 2019.

[18] N. A. Bianco, S. H. Collins, K. Liu, and S. L. Delp, "Simulating the effect of ankle plantarflexion and inversion-eversion exoskeleton torques on center of mass kinematics during walking," *PLoS Computational Biology*, vol. 19, no. 8, p. e1010712, 2023.